

Depth-resolved strain measurements in polycrystalline materials by energy-variable X-ray diffraction

E. Zolotoyabko,^{a*} B. Pokroy^a and J. P. Quintana^b

^aDepartment of Materials Engineering, Technion – Israel Institute of Technology, Haifa 32000, Israel, and ^bDND-CAT Research Center, Northwestern University, APS/ANL Sector 5, Building 432A, 9700 South Cass Avenue, Argonne, IL 60439-4857, USA. E-mail: zloto@tx.technion.ac.il

An energy-variable synchrotron diffraction technique is being established as a novel method for the depth-resolved measurement of residual strains in polycrystalline structures. An analytic expression for the diffraction profile is obtained by taking into account the instrument misalignment, change of the height of an incident X-ray beam with energy, and penetration of X-rays into the sample depth. It is shown that the maximum diffraction intensity recorded in the detector is coming from a certain depth beneath the surface of the sample, the depth being energy-dependent. This finding opens a way for precise strain measurements with high depth resolution by changing the X-ray energy in small enough steps. An experimental example, residual strain measurements across an alumina/zirconia multilayer, demonstrates the capability of the method.

Keywords: X-ray diffraction; residual strains; microstructure.

1. Introduction

Very recently we have started to explore the capability of energy-variable diffraction (EVD) on synchrotron beamlines to provide depth-resolved microstructural characteristics in polycrystalline structures (Zolotoyabko & Quintana, 2002*a,b*, 2003). In that method, precise energy variation is accomplished by a computer-controlled double-crystal monochromator, which provides the desirable changes in the X-ray penetration depth. We demonstrated that energy-dependent diffraction intensities could be used to study preferred orientation with depth resolution (Zolotoyabko & Quintana, 2002*a*), while diffraction profile analysis (profile broadening) at variable X-ray energy supplies depth-resolved information on grain size and microstrain fluctuations (Zolotoyabko & Quintana, 2002*b*, 2003). At the same time it turned out that the depth-resolved macro- or residual strains could not be derived directly from the diffraction peak positions measured. Even in free-of-strain samples we found small but systematic deviations of the measured Bragg angles from those expected in the case of undistorted lattice parameters. For example, in powdered alumina samples in the energy range 7–40 keV, the angular deviations, $\Delta 2\Theta$, reached 0.03° , a fact that complicates the precise strain determination below 10^{-3} . In order to overcome this difficulty we used an empirically derived correction function, which we called the ‘chromatic aberration’ of the instrument (Zolotoyabko & Quintana, 2003). That function was determined by measuring the energy-dependent peak positions with a standard sample (free of residual strains), but at the stage reported its origin remained unclear.

In this paper we develop a comprehensive analysis of the chromatic aberration in EVD. Chromatic aberration originates in the initial misalignment of the diffraction instrument, which cannot be totally eliminated, and in energy-dependent changes in the height of the X-ray beam issuing from the double-crystal monochromator. The

analytic description of the chromatic aberration effect allowed us to realise that under appropriate conditions it can be used for strain measurements with high depth resolution. This finding opens the way for a novel method of depth-resolved strain analysis by EVD.

2. The chromatic aberration effect

We begin our analysis by calculating the height of the synchrotron beam after the double-crystal monochromator, as a function of the X-ray energy, in standard vertical-scattering geometry. It is known that the X-ray beam rises with energy. In order to obtain an analytic expression in appropriate notations, let us consider a white beam entering a double-crystal monochromator at height H_0 above the ground level (see Fig. 1). The gap (normal to the surface) between crystals is designated G , and the energy-dependent Bragg angle Θ_m . It is easily shown that the outgoing beam is shifted upwards by ΔH with respect to an incident beam,

$$\Delta H = 2G \cos \Theta_m. \quad (1)$$

The height difference, δH , measured at some energy, $E > E_0$, relative to the initial energy, E_0 , is

$$\delta H = \Delta H(E) - \Delta H(E_0) = 2G[\cos \Theta_m(E) - \cos \Theta_m(E_0)]. \quad (2)$$

When analyzing the angular positions of the diffraction peaks in polycrystalline materials, synchrotron radiation is well approximated by parallel rays; hence the ray optics approach is adequate. The monochromated X-rays of energy E , entering a sample at point A (the height $H = H_0 + \Delta H$), penetrate some depth Z (counted normal to the surface) within the sample, and in point B are scattered towards the detector, the energy-dependent double Bragg angle being 2Θ (see Fig. 2). The scattered X-rays cross the detector circle at point M . If B does not coincide with the center of rotation C of the detector, the detector reading will differ from the true angle of diffraction, 2Θ , by some extra quantity, α , which, in fact, is energy-dependent (at least *via* ΔH and Z). The value of α determines the chromatic aberration of the instrument.

In order to calculate α , let us plot the straight line, CN , which is parallel to BM , passes through the detector’s center of rotation, C , and crosses the detector circle at point N . Evidently,

$$\alpha(Z) = MN/R, \quad (3)$$

where R is the distance between the sample and the receiving slit of the detector and MN is an arc length (see Fig. 2). Since practically the α values are very small ($\alpha \ll 1$), in further analysis we will not distinguish between arcs and their segments. It is worth noting that, even when an instrument is ideally aligned at a given energy (points B and C coinciding), the misalignment emerges when the energy is changed.

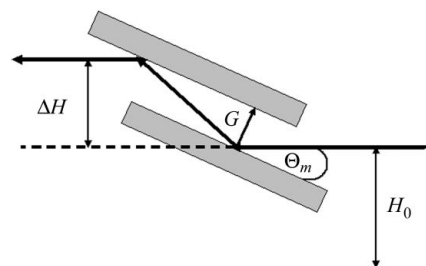


Figure 1
Change in the height of the X-ray beam after the double-crystal monochromator.

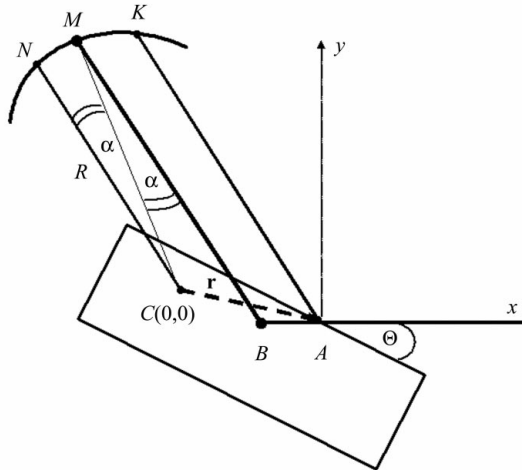


Figure 2
Sketch of the chromatic aberration effect.

Let us first calculate the value of $\alpha(0)$ at $Z = 0$, which depends on the vector $\mathbf{r}(\eta, \xi)$ connecting points A and C . The horizontal projection, η , is parallel to the direction of an incident beam (x axis), the ξ projection is parallel to the vertical direction (y axis) (see Fig. 2). The origin of the coordinate system is placed at point $C(0, 0)$. The diffracted beam crosses the detector circle at point K , hence

$$\alpha(0) = KN/R. \quad (4)$$

The equation for CN is

$$y = -x \tan 2\Theta \quad (5)$$

and for AK

$$y = (\xi + \eta \tan 2\Theta) - x \tan 2\Theta. \quad (6)$$

Calculating the points of intersection of these lines with the detector's circle,

$$x^2 + y^2 = R^2, \quad (7)$$

yields the KN value

$$KN = \xi \cos 2\Theta + \eta \sin 2\Theta, \quad (8)$$

and, hence,

$$\alpha(0) = KN/R = (\xi \cos 2\Theta + \eta \sin 2\Theta)/R. \quad (9)$$

If the scattering event takes place at some depth, Z , beneath the sample surface, this leads to the reduction of the η projection by the segment, $AB = Z/\sin \Theta$. Correspondingly,

$$\alpha(Z) = (\xi \cos 2\Theta - 2Z \cos \Theta + \eta \sin 2\Theta)/R. \quad (10)$$

In order to find the change in the α value as a function of energy, we have to take into account both the turning of the sample about its center of rotation (to fit the energy-dependent Bragg angles, Θ) and the above-mentioned energy-dependent changes in the height of the incident beam.

Let us assume that the sample's center of rotation is located at point $O(X, Y)$ of the sample surface, *i.e.* it is displaced from the detector's center of rotation by segments X and Y along the x and y axes, respectively (see Fig. 3, in which the positive directions of the coordinate axes are indicated by arrows). To simplify the geometrical problem and come closer to our experimental conditions, let us also assume that the alignment of the instrument is accomplished at the lowest energy, E_0 , and that at this energy the incident beam is

crossing the sample's center of rotation, *i.e.* point O . Naturally, these restrictions can be easily removed, if needed. It follows immediately from Fig. 3 that, at $E = E_0$,

$$\begin{aligned} \xi_0 &= Y, \\ \eta_0 &= X. \end{aligned} \quad (11)$$

Using (10) yields

$$\alpha_o(Z) = (1/R)(Y \cos 2\Theta_o + X \sin 2\Theta_o - 2Z_o \cos \Theta_o), \quad (12)$$

where Z_o and Θ_o are the X-ray penetration depth and Bragg angle, respectively, at $E = E_0$. At $E > E_0$,

$$\begin{aligned} \alpha(Z) &= (1/R)(-\delta H + Y \cos 2\Theta + X \sin 2\Theta - 2Z \cos \Theta) \\ &= \beta - [(2Z \cos \Theta)/R], \end{aligned} \quad (13)$$

where $\beta = (-\delta H + Y \cos 2\Theta + X \sin 2\Theta)/R$ is the Z -independent part of the angular deviation in (13).

The measurable parameter is the difference, $\Delta\alpha = \alpha(Z) - \alpha(Z_o)$,

$$\begin{aligned} \Delta\alpha &= (1/R)[-\delta H + Y(\cos 2\Theta - \cos 2\Theta_o) + X(\sin 2\Theta - \sin 2\Theta_o) \\ &\quad - 2Z \cos \Theta + 2Z_o \cos \Theta_o]. \end{aligned} \quad (14)$$

Some examples of the energy-dependent $\Delta\alpha$ functions at $Z = 0$ and different values of X, Y are shown in Fig. 4. The plots in Fig. 4 represent the chromatic aberration in EVD, depending on the experimental parameters. A question regarding the Z values in (13) and (14) requires deeper investigation and is treated in the following section.

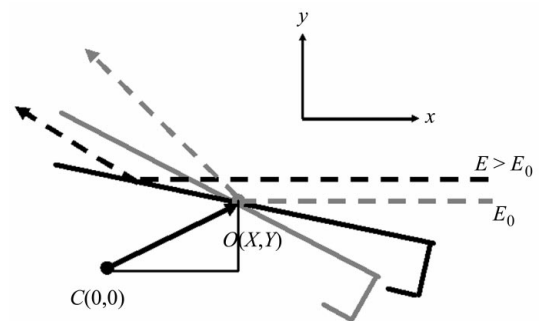


Figure 3
X-ray trajectories at different energies.

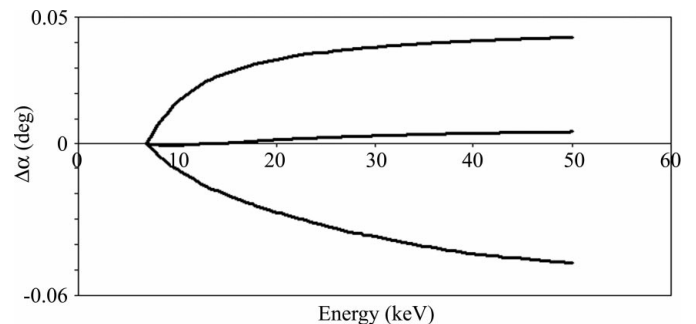


Figure 4
Selected examples of the chromatic aberration function calculated using (14) for $Z = 0$ and the following parameters X, Y : bottom curve, $X = 1$ mm, $Y = 1$ mm; middle curve, $X = -0.6$ mm, $Y = 0$; upper curve, $X = -1$ mm, $Y = 2.2$ mm.

3. Depth sensitivity in EVD measurements

It turned out that the ‘Z problem’ is quite fundamental and is directly related to the depth sensitivity of the EVD technique. In fact, in the conventional X-ray diffraction analysis of polycrystalline materials (Warren, 1990) the diffraction signal is considered as being detected from an entire sample thickness. It is assumed that the X-rays emanating from the different sub-layers are recorded with equal probabilities within the detector. The depth dependence of the diffraction intensity is introduced *via* an exponentially decreasing weight function, $W = \exp(-Z/\Lambda)$, which takes into account the in-depth attenuation of the X-ray flux. The characteristic depth,

$$\Lambda = (\sin \Theta)/2\mu, \quad (15)$$

is determined by the Bragg angle, Θ , and the linear absorption coefficient, μ , both of which are energy-dependent. The diffraction profile is effectively collected from a layer a few Λ thick (the thickness being counted from the sample surface) and hence the depth sensitivity is rather poor.

The situation is drastically changed for the diffracted quasi-parallel synchrotron beam, which has an offset, $\alpha(Z)$, with respect to the axis of the detector’s collimating system (see Fig. 2). In fact, it follows from (13) that the diffracted X-rays issuing from various depths, Z , enter the detector at different angles, α . They will therefore not register there with equal probability. Under appropriate conditions ($\beta > 0$ is a necessary one), an increase in the probability of registration with increasing depth owing to decreasing α can overcome the reduction in intensity owing to the X-ray attenuation. In that case, the maximum diffraction intensity registered in the detector originates at a certain depth beneath the surface. We stress that this characteristic depth is energy-dependent, which generally provides high depth resolution to the strain measurements if the energy steps applied are small enough. The requirement for positive β could be justified by recalling that the probability of the X-ray registration in the detector depends on $\alpha^2 = \{\beta - [2Z(\cos \Theta)/R]\}^2$ [see (13)]. Since in our analysis only positive Z values (*i.e.* pointed from the surface to the crystal bulk) make sense, then a decrease of the parameter $\alpha^2 = \{\beta - [2Z(\cos \Theta)/R]\}^2$ (*i.e.* an increase of the registration efficiency with increasing Z) can only be achieved for $\beta > 0$. In the case where $\beta < 0$, the parameter α^2 is always growing with Z .

Let us support these qualitative considerations by the direct simulation of the diffraction profile, *i.e.* the dependence of the measured diffraction intensity, $I(\Delta 2\Theta)$, on the deviation, $\Delta 2\Theta$, of the detector angle from the exact Bragg position, 2Θ . Let us assume that the probability of registration in the detector is described by the Gaussian function with the dispersion σ ,

$$P = [1/\sigma(2\pi)^{1/2}] \exp\{-[\Delta 2\Theta - \alpha(Z)]^2/2\sigma^2\}. \quad (16)$$

This is a rather standard approximation to describe the transmission function of the receiving slit of diffraction instruments. In this approximation, the dispersion σ is related to the receiving slit width, D , as

$$\sigma = D/[2R(2 \ln 2)^{1/2}] \simeq D/2R.$$

In our experiments described in §4, $R \simeq 1$ m and $D = 1$ mm, so $\sigma \simeq 5 \times 10^{-4}$.

By taking into account the exponential attenuation of the X-ray flux with depth, $W = \exp(-Z/\Lambda)$, the diffraction intensity, $I(\Delta 2\Theta)$, can be expressed as

$$I(\Delta 2\Theta) = \int_0^\infty (SWP) dZ, \quad (17)$$

where S is the scattering power of the material. If the $S(Z)$ function is slowly changed on the distances of the order of Λ , we can take $S(Z)$ out of integral (17) and obtain

$$\begin{aligned} I(\Delta 2\Theta) &= \frac{S}{\sigma(2\pi)^{1/2}} \int_0^\infty dZ \exp\left(\frac{-Z}{\Lambda}\right) \exp\left\{\frac{-[\Delta 2\Theta - \alpha(Z)]^2}{2\sigma^2}\right\} \\ &= \frac{S}{\sigma(2\pi)^{1/2}} \int_0^\infty dZ \exp\left(\frac{-Z}{\Lambda}\right) \\ &\quad \times \exp\left\{\frac{-[\Delta 2\Theta - \beta + (2Z \cos \Theta/R)]^2}{2\sigma^2}\right\}. \end{aligned} \quad (18)$$

To integrate over Z in (18), let us complete the square in the exponent,

$$\begin{aligned} \frac{1}{2\sigma^2} \left(\Delta 2\Theta - \beta + \frac{2Z \cos \Theta}{R} \right)^2 + \frac{Z}{\Lambda} = \\ - \frac{R}{2\Lambda \cos \Theta} \left(\Delta 2\Theta - \beta + \frac{\sigma^2 R}{4\Lambda \cos \Theta} \right) \\ + \frac{1}{2} \left[\frac{2Z \cos \Theta}{\sigma R} + \left(\frac{\Delta 2\Theta}{\sigma} - \frac{\beta}{\sigma} + \frac{\sigma R}{2\Lambda \cos \Theta} \right) \right]^2. \end{aligned} \quad (19)$$

Integral (18) is then reduced to

$$\begin{aligned} I(\Delta 2\Theta) &= \frac{RS \exp[(\Delta 2\Theta - \beta)R/(2\Lambda \cos \Theta)] \exp[\sigma^2 R^2/(8\Lambda^2 \cos^2 \Theta)]}{2(2\pi)^{1/2} \cos \Theta} \\ &\quad \times \int_{t_0}^\infty \exp(-t^2/2) dt \end{aligned} \quad (20)$$

where

$$\begin{aligned} t &= (2Z \cos \Theta/\sigma R) + t_0, \\ t_0 &= (\Delta 2\Theta/\sigma) - (\beta/\sigma) + \sigma R/(2\Lambda \cos \Theta). \end{aligned} \quad (21)$$

As we have already mentioned, for estimations one can take $R \simeq 1$ m, $\Lambda = 10$ – 100 μm , $\sigma \simeq \beta \simeq 5 \times 10^{-4}$, which yields $\beta/\sigma \simeq 1$ and $\sigma R/2\Lambda \cos \Theta \gg 1$. Because we are interested in the peak position, then $\Delta 2\Theta/\sigma \leq 1$. Substituting the above estimations into (21) yields $t_0 \gg 1$. Using the known asymptotic of the error function at large t_0 values,

$$\int_{t_0}^\infty \exp(-t^2/2) dt \simeq [\exp(-t_0^2/2)]/t_0, \quad (22)$$

yields an analytical expression for the diffraction profile near the Bragg angle,

$$\begin{aligned} I(\Delta 2\Theta) &= \frac{(\sigma R)S}{2(2\pi)^{1/2} \cos \Theta} \exp[-(\Delta 2\Theta - \beta)^2/2\sigma^2] \\ &\quad \times [\Delta 2\Theta - \beta + \sigma^2 R/(2\Lambda \cos \Theta)]^{-1}. \end{aligned} \quad (23)$$

Maximum intensity is achieved at angular deviation $(\Delta 2\Theta)_p$, satisfying the condition

$$\frac{\partial I}{\partial(\Delta 2\Theta)} = 0, \quad (24)$$

which yields

$$(\Delta 2\Theta)_p = \beta - (2\Lambda \cos \Theta)/R. \quad (25)$$

By comparing (13) and (25), it can be concluded that the maximum intensity recorded in the detector comes from the depth

$$Z_p = \Lambda. \quad (26)$$

This result quantitatively explains the depth sensitivity of the method and hence is of principal importance to the establishment of the EVD technique. It should be emphasized that (23) determines the actual shift in the peak position rather than some distortion of the profile's left-hand tail only, as is observed in conventional powder diffraction profiles taken from transparent samples (see *e.g.* Ida & Kimura, 1999). The depth resolution of EVD will primarily depend on how precisely an angular position of the diffraction peak can be determined. This can be done very accurately from the diffraction profile fittings, since we are using intense quasi-parallel synchrotron radiation and have no problems with counting statistics.

By combining (14) and (26), first, we are able to complete an analysis of the chromatic aberration effect,

$$\Delta\alpha = (1/R)[- \delta H + Y(\cos 2\Theta - \cos 2\Theta_o) + X(\sin 2\Theta - \sin 2\Theta_o) - 2\Lambda \cos \Theta + 2\Lambda_o \cos \Theta_o], \quad (27)$$

A comparison of the calculated and the measured $\Delta\alpha$ functions is shown in Fig. 5. In these measurements we used the (104) reflection of a sample of powdered alumina (NIST standard). The agreement between calculated and measured data is fairly good. Note that the influence of depth, Z , on the chromatic aberration is clearly revealed in the form of a gradual reduction in the $\Delta\alpha(E)$ values at higher energies, which is absent in calculations for $Z = 0$ (see Fig. 4). By applying (27) to reference data we are able to extract the instrument parameters X , Y (for a given alignment procedure) and use them to precisely measure the diffraction peak positions of the investigated samples. Besides that, such measurements may serve to perform very accurate instrument alignments, if needed.

Changing the X-ray energy and the depth of the X-ray penetration, Λ , by controlled steps allows us directly to obtain depth-resolved residual strains. We stress that in this method we avoid inverse Laplace transformation of the measured parameters in the spatial domain, as was proposed, for example, in the 'scattering vector mode' (Genzel, 1996). Concerning depth resolution, our estimations show that, as a rule, energy steps of 100 eV provide depth variations on a sub- μm scale. Working near an absorption edge, the in-depth steps may be as small as a few tens of nm. These numbers are much better than the depth resolution obtained by using energy-dispersive X-ray diffraction of white synchrotron radiation (see *e.g.* Hall *et al.*, 1998; Korsunsky *et al.*, 2002).

4. Experimental example

In order to illustrate the capability of the method, we applied it to the measurement of residual strains within an $\text{Al}_2\text{O}_3/\text{ZrO}_2$ multilayer consisting of 90 layers with nominal thickness of 30 and 20 μm for

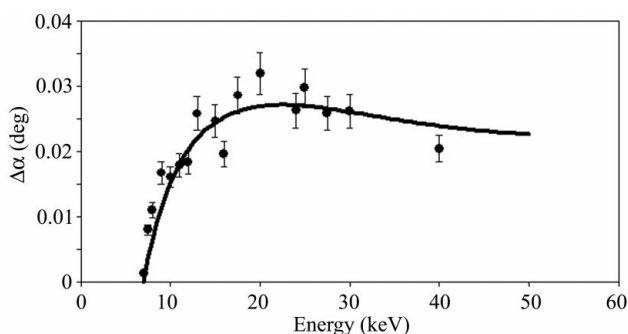
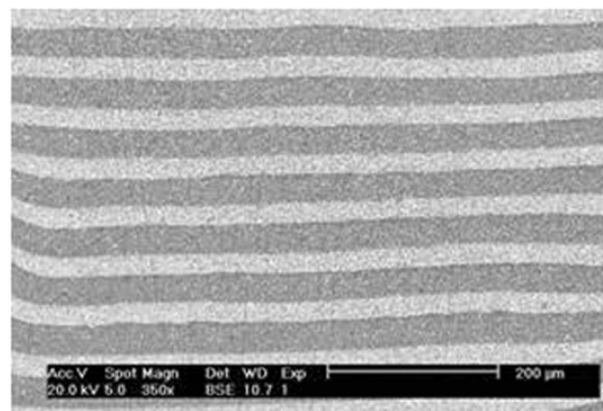


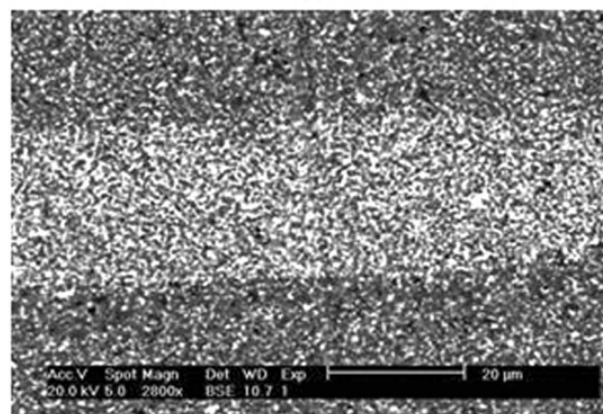
Figure 5 Comparison between the measured (dotted line) and the calculated (solid line) chromatic aberration, as a function of the X-ray energy. The solid line was calculated using (27) and $X = -1$ mm and $Y = 2.2$ mm.

alumina and zirconia, respectively, produced by electrophoretic deposition followed by sintering for 2 h at 1823 K (Gal-Or *et al.*, 1999). The basis of the deposition method can be found *e.g.* in Sarkar & Nicholson (1996). These laminates have improved mechanical properties and can serve as structural ceramics for applications requiring high fracture toughness. Alternating alumina and zirconia layers are clearly seen in SEM cross sections (see Fig. 6a). In fact, some amount of alumina particles had been added to the zirconia layers and *vice versa* in the deposition stage (Gal-Or *et al.*, 1999), in order to reduce the thermal stresses caused by the different thermal expansion coefficients, *viz.* $13.5 \times 10^{-6} \text{ K}^{-1}$ of zirconia and $8.5 \times 10^{-6} \text{ K}^{-1}$ of alumina. The zirconia particles in an alumina layer and the alumina particles in a zirconia layer are discernible in SEM images under higher magnification (see Fig. 6b). Inclusions of a secondary phase in the matrix are the sources of the inhomogeneous residual strains influencing mechanical properties.

In order to obtain depth dependence of the strain component, ε , normal to the sample's surface, we measured the (012) Al_2O_3 and (101) ZrO_2 diffraction profiles in the energy range 7–40 keV. Residual strains as a function of the X-ray penetration depth (see Fig. 7) were extracted from the measured diffraction peak position by applying the chromatic aberration correction, as was explained in previous sections. Owing to the presence of Zr atoms, which have the K absorption edge at $E = 17.997$ keV, the effective X-ray penetration depth, $\Lambda(E)$, through the alumina/zirconia multilayer at energies used is confined to 6–34 μm . Because of this limited penetration, the strain sensitivity is enhanced in the interface region near 30 μm . In



(a)



(b)

Figure 6 SEM cross sections at (a) lower and (b) higher magnifications. In these images, zirconia particles appear bright, while alumina appear dark.

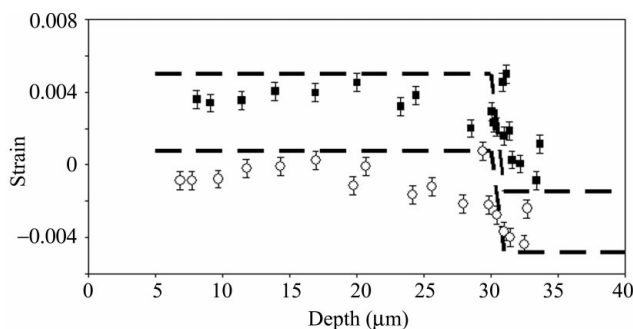


Figure 7
Depth-dependent residual strains measured in zirconia (squares) and alumina (circles) particles. The dashed lines represent calculated strain levels.

the reported measurements we applied energy steps in a keV range, resulting in depth changes of 100–400 nm near the interface, which were fine enough to follow strain modifications in this region (see Fig. 7). We repeat that, from an energy point of view, the depth steps can be easily reduced ten times if necessary.

The major source of residual strains in our system is the difference in thermal expansion coefficients of the components. On this basis, we expect that, after cooling from 1823 K to room temperature, the zirconia particles in the alumina matrix are stretched, while the alumina particles in the zirconia matrix shrink. The depth-dependent strains obtained in zirconia and alumina particles (see Fig. 7) support these considerations.

In fact, zirconia particles in the alumina layer (which is the first one in the stack) are under tensile stresses ($\epsilon > 0$) (see region $\Lambda < 30 \mu\text{m}$ in Fig. 7), as was deduced from the (101) ZrO_2 diffraction peak positions. At $\Lambda > 30 \mu\text{m}$, *i.e.* in the zirconia layer itself, the strain value within the zirconia particles diminishes to some low level, which depends on forces acting on the alumina/zirconia interface. At the same time, when analyzing the (012) Al_2O_3 diffraction profiles, residual strains in the alumina matrix ($\Lambda < 30 \mu\text{m}$) were found to be close to zero (see Fig. 7). Alumina particles in the zirconia matrix (at $\Lambda \geq 30 \mu\text{m}$) are, as expected, under compressive stresses ($\epsilon < 0$) (see Fig. 7).

The dashed lines in Fig. 7 represent the strain levels calculated in the framework of a simple model for local stresses. In this model the local thermal stress is a result of two contributions: biaxial stress arising at the alumina/zirconia interface (see *e.g.* van Heerden *et al.*, 1996), and isotropic hydrostatic pressure around an isolated particle of the secondary phase within a homogeneous matrix (see *e.g.* Chawla, 1998). The normal stress component is assumed to be zero across the entire multilayer. Simulated strain values are in reasonable agreement with the experimental data. At the same time, we have to acknowledge that in the alumina layer ($\Lambda < 30 \mu\text{m}$) the measured strains are a little lower than theoretical predictions. Further studies are needed to shed additional light on the discrepancies observed.

5. Summary

The analysis developed allowed us to quantitatively describe the chromatic aberration effect in EVD. Using the appropriate correction function opens the way for a novel strain analysis with high depth resolution *via* precise measurements of energy-dependent diffraction

peak positions. We used the procedure developed in order to study residual strains across the alumina/zirconia multilayer and found significant strain modifications near the alumina/zirconia interface. To the best of our knowledge there is no established method to the non-destructive measurement of the depth-resolved strains with a sub- μm resolution at a depth of 30 μm beneath the surface of the sample.

Finally, we would like to make some general remarks concerning the restrictions of the EVD technique. Strictly speaking, the developed mathematical analysis is valid for a homogeneous and infinite medium. In the case of inhomogeneous materials, in which the scattering power notably varies with depth, the mathematical equations should be rewritten to take into account the structure of specific materials systems. However, the main principle, *viz.* that the maximum of diffraction intensity registered in the detector originates at certain depth, which is energy-dependent, remains with no change. The characteristic depth value could be different from Λ (being determined by another equation or numerical procedure), but depth-dependent strain modifications will still be visible, as is shown in the current study of ceramic multilayers. Further investigation is needed in order to evaluate the real potential of the developed technique.

The experimental part of this work was performed at the DuPont–Northwestern–Dow Collaborative Access Team (DND-CAT) Synchrotron Research Center located at Sector 5 of the Advanced Photon Source. DND-CAT is supported by E. I. DuPont de Nemours & Co., the Dow Chemical Company, the US National Science Foundation through grant DMR-9304725, and the State of Illinois through the Department of Commerce and the Board of Higher Education's Grant IBHE HECA NWU 96. Use of the Advanced Photon Source was supported by the US Department of Energy, Basic Energy Sciences, Office of Energy Research, under contract No. W-31-102-Eng-38. We thank Dr Lea Gal-Or for supplying the alumina/zirconia multilayers and discussing their properties. One of the authors (EZ) would like to thank the Fund for the Promotion of Research at the Technion and the Israel Science Foundation founded by the Israel Academy of Sciences and Humanities for financial support.

References

- Chawla, K. K. (1998). *Composite Materials: Science and Engineering*, 2nd ed. New York/Berlin/Heidelberg: Springer-Verlag.
- Gal-Or, L., Brandon, D., Goldner, R., Cherniak, L., Perlin, L., Sezin, N. & Liubovich, S. (1999). US Patent 5919347.
- Genzel, Ch. (1996). *Phys. Status Solidi A*, **156**, 353–363.
- Hall, C., Barnes, P., Cockcroft, J. K., Colston, S. L., Hausermann, D., Jacques, S. D. M., Jupe, A. P. & Kunz, M. (1998). *Nucl. Instrum. Methods Phys. Res. B*, **140**, 253–257.
- Heerden, D. van, Zolotoyabko, E. & Shechtman, D. (1996). *J. Mater. Res.* **11**, 2825.
- Ida, T. & Kimura, K. (1999). *J. Appl. Cryst.* **32**, 982–991.
- Korsunsky, A. M., Collins, S. P., Owen, R. A., Daymond, M. R., Achioui, S. & James, K. E. (2002). *J. Synchrotron Rad.* **9**, 77–81.
- Sarkar, P. & Nicholson, P. S. (1996). *J. Am. Ceram. Soc.* **79**, 1987–2002.
- Warren, B. E. (1990). *X-ray Diffraction*. New York: Dover.
- Zolotoyabko, E. & Quintana, J. P. (2002a). *Rev. Sci. Instrum.* **73**, 1663–1667.
- Zolotoyabko, E. & Quintana, J. P. (2002b). *J. Appl. Cryst.* **35**, 594–599.
- Zolotoyabko, E. & Quintana, J. P. (2003). *Nucl. Instrum. Methods B*, **200**, 382–389.